ISSN 1392-1207. MECHANIKA. Vol. 32, No. 5, 2026: 377–388

Design and Performance Investigation of a Novel Composite Sealing Structure for Plunger Pumps

Xianjun ZHOU*, Jiajun ZHANG*, Feng LI, Haoran WANG*, Yan WANG*****

**School of Mechatronic Engineering, China University of Petroleum (East China), Qingdao 266580, China, E-mail: zhouxianjun@upc.edu.cn*

***Shengli Oilfield Technical Testing Center, Dongying 257000, China, E-mail: 19854283085@qq.com*

****Haier Group, Qingdao, 266103, China, E-mail: 1611657359@qq.com*

https://doi.org/10.5755/j02.mech.45655

1. Introduction

Plunger pumps for oilfield service operate under harsh conditions of high pressure, high stroke frequency and severe corrosion [1]. Packing seals are commonly adopted as the main sealing form for such pumps [2, 3]. A packing seal generates sealing performance via packing compression; elastic deformation makes the packing closely fit the reciprocating plunger. Continuous friction takes place between the packing and reciprocating plunger during operation. Intense heat is produced under high-speed working conditions, resulting in aging and adhesion of the packing. Consequently, the service life of the packing seal is shortened, and seal failure may even occur [4].

The typical existing packing seal configurations for plunger pumps consist of conventional sealing structures, spring-loaded sealing structures and reverse loading sealing structures. Most designs only adjust the assembly mode of sealing elements and the structural form of the stuffing box. However, the majority of these structures cannot withstand pressure up to 40 MPa, and are unable to satisfy the demands of reliable sealing and long service life [5].

In engineering practice, single homogeneous materials are widely used as packing media [6, 7]. Such sealing elements exhibit rapid wear, accompanied by short service life and frequent replacement [8, 9].

As a vital pressure-reduction component of labyrinth regulating valves, the labyrinth seal possesses internal flow characteristics that directly determine the pressure drop capability and flow performance of the valve [10, 11]. Numerous scholars have conducted extensive investigations into the pressure reduction characteristics of labyrinth channels arranged inside valve bodies. Nevertheless, few studies focus on applying labyrinth seals to water injection plunger pumps.

At present, limited research at home and abroad addresses combined sealing structures for plunger pumps. By integrating labyrinth seals with packing seals, the front-mounted labyrinth structure can reduce the pressure acting on downstream packing, extend the service life of packing seals, and further prolong the service life of the whole sealing system of plunger pumps. For this reason, the present work carries out research on the structural design of combined sealing assemblies for plunger pumps.

To overcome the problems of easy leakage and short service life existing in conventional packing seals of plunger pumps, this paper proposes a novel composite sealing scheme. A trapezoidal labyrinth seal is arranged on the high-pressure side, and a stepped inner stuffing box is adopted inside the packing housing to realize the combination of labyrinth seal and packing seal. Numerical simulation is utilized to investigate the flow characteristics of the trapezoidal labyrinth seal, and the effects of structural parameters of V-shaped packing on packing sealing performance are analyzed. Finally, experiments are implemented to verify the above research findings.

2. Composite Sealing Structure of Plunger Pump

The composite sealing structure of the plunger pump is composed of two parts: 1. design of the front-mounted labyrinth sealing structure; 2. design of the packing sealing structure.

A three-cylinder plunger pump with model 3ZB180-10/40, which is widely used in oilfields, is selected as the research object for structural dimension design of the composite sealing structure. This pump delivers clean water and oilfield produced water, and is equipped with a reciprocating plunger with a diameter of 41 mm and a length of 400 mm to match the actual service conditions.

2.1. Front-mounted labyrinth sealing structure

The commonly adopted tooth profiles of labyrinth seals at present include rectangular, trapezoidal, triangular and straight triangular types. To analyze the flow characteristics of labyrinth seals with the four tooth profiles, Fluent software is used to conduct numerical simulation on the internal flow field of each labyrinth structure, and the simulation results are presented in Figs. 1, 2 and 3.

It can be seen from Fig. 1 that the difference in total pressure drop among the four tooth profiles is small, and the trapezoidal tooth profile 2 achieves the maximum pressure drop. The fluid pressure loss of all four structures mainly occurs after the fluid passes through the labyrinth grooves; the fluid pressure drops sharply when the medium flows from the groove of the previous tooth to the groove of the subsequent tooth.

Figs. 2 and 3 show that at the junction of the sealing cavity and the downstream sealing clearance, part of the liquid flows directly into the next tooth groove along the smooth flow channel, while the remaining liquid flows backward to form vortices. The flow velocity in the sealing clearance is significantly higher than that inside the sealing cavity. Compared with the other three tooth profiles, tooth profile 2 generates sufficient turbulent flow to strengthen fluid energy dissipation and impose prominent flow resistance on the medium. The rectangular tooth profile 1 fails

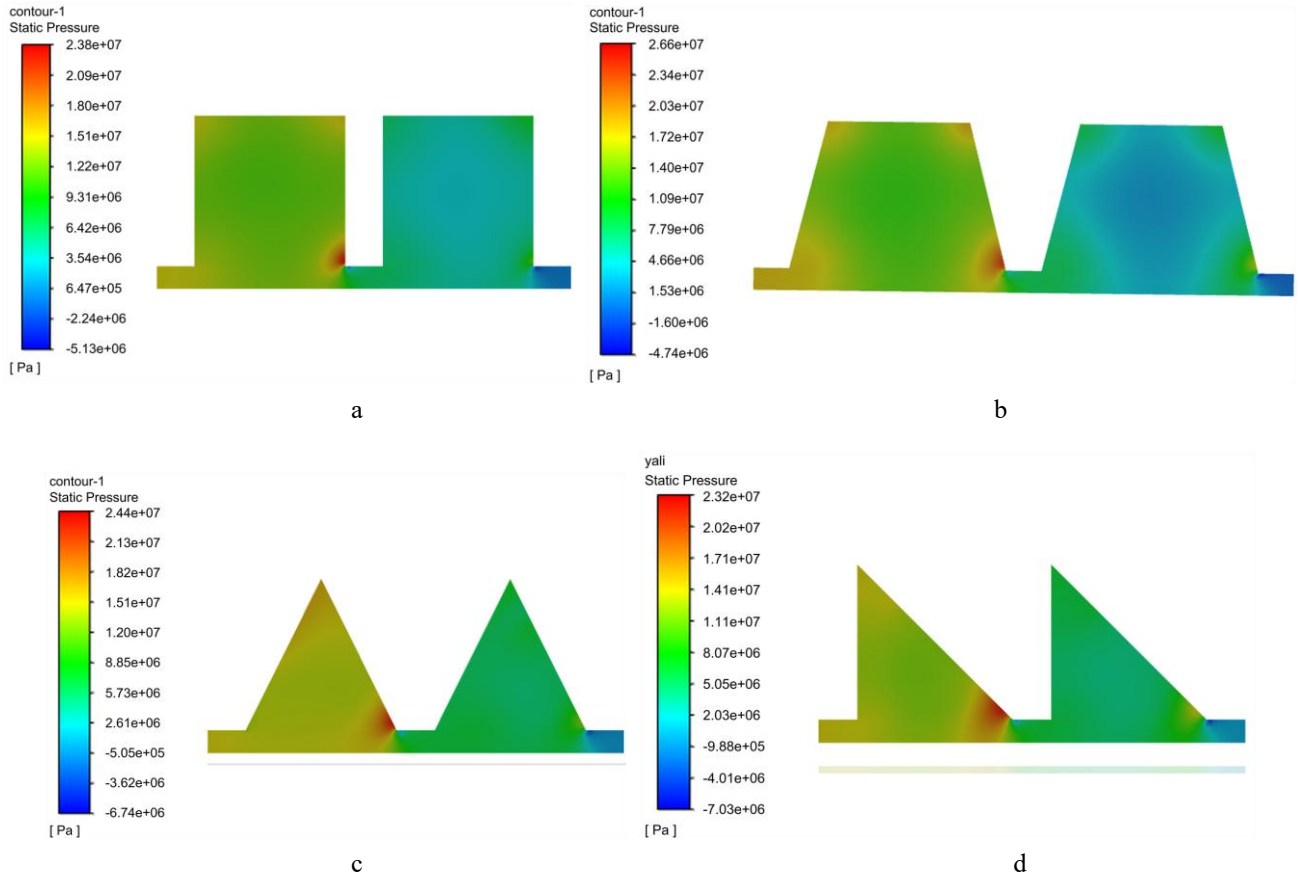

Fig. 1 Pressure contour: a – rectangular tooth profile 1, b – trapezoidal tooth profile 2, c – triangular tooth profile 3, d – straight triangular tooth profile 4

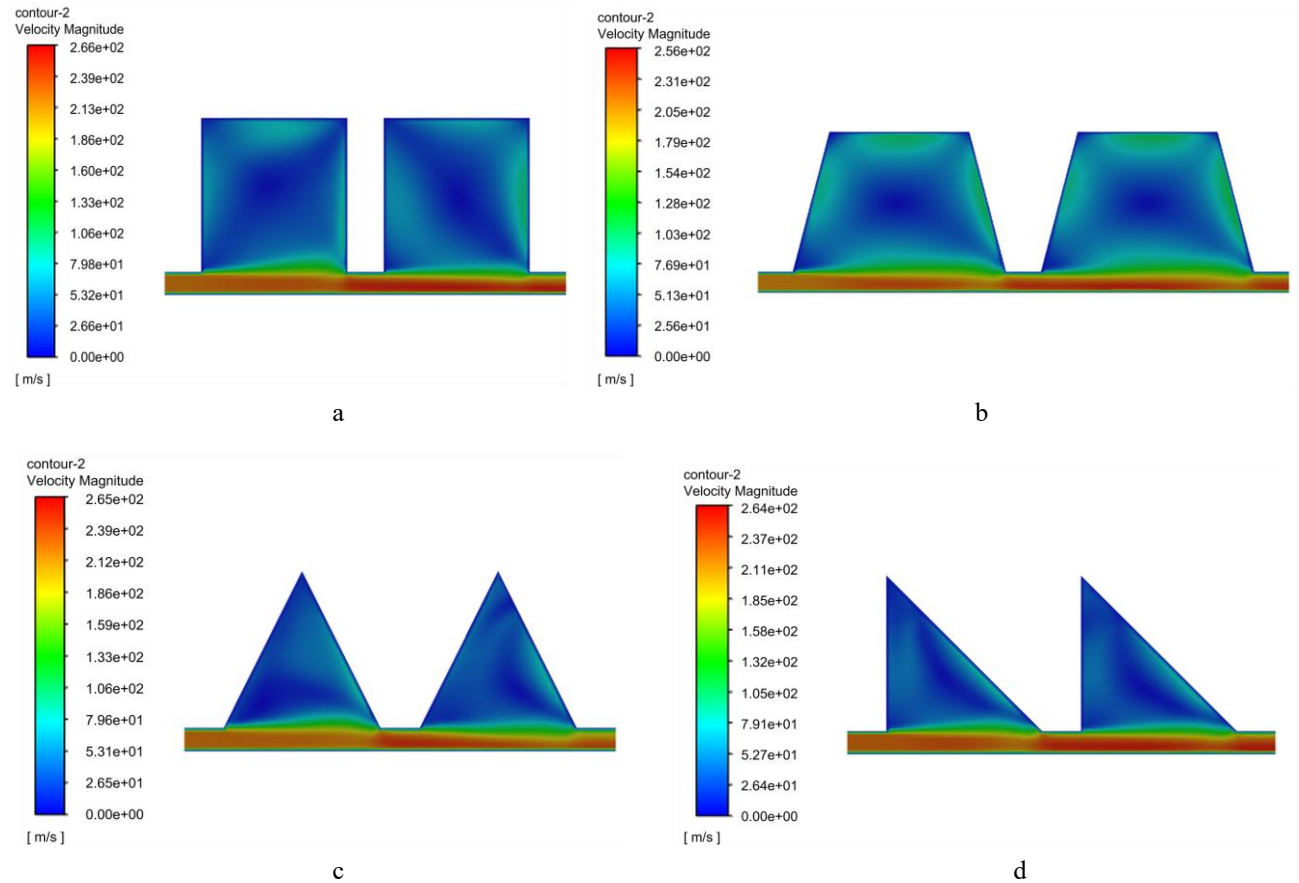

Fig. 2 Velocity contour: a – rectangular tooth profile 1, b – trapezoidal tooth profile 2, c – triangular tooth profile 3, d – straight triangular tooth profile 4

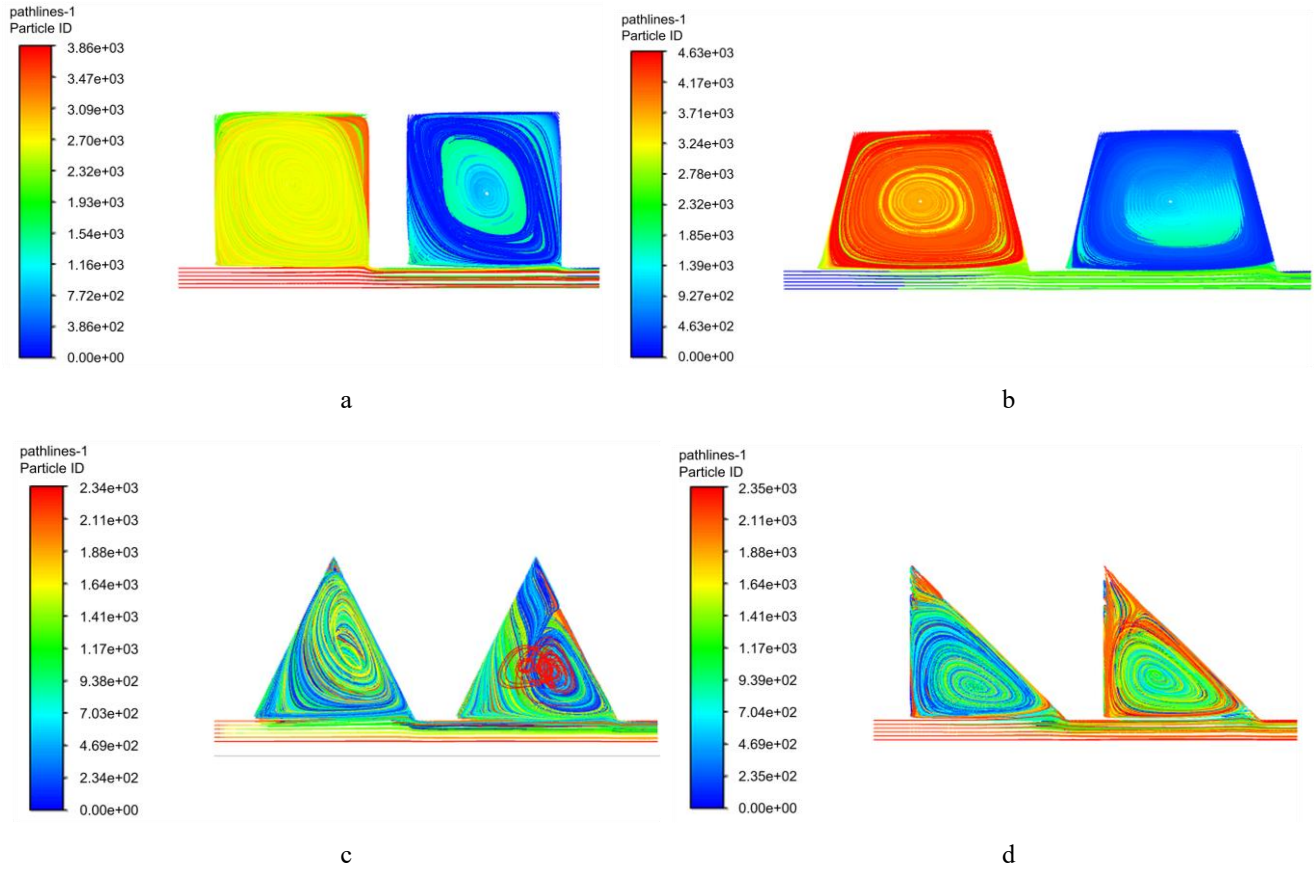

Fig. 3 Fluid trajectory diagram: a – rectangular tooth profile 1, b – trapezoidal tooth profile 2, c – triangular tooth profile 3, d – straight triangular tooth profile 4

to form effective vortices and thus provides limited flow obstruction, while the performance of tooth profiles 3 and 4 falls between the above two types.

In summary, the trapezoidal tooth profile can produce a large total pressure drop and maintain a stable pressure dissipation capacity along the flow path.

Considering the high stroke frequency and high working pressure of the three-cylinder plunger pump, as well as the manufacturability and practical processing requirements, a trapezoidal labyrinth clearance structure is proposed in this paper, and its structural drawings are shown in Fig. 4.

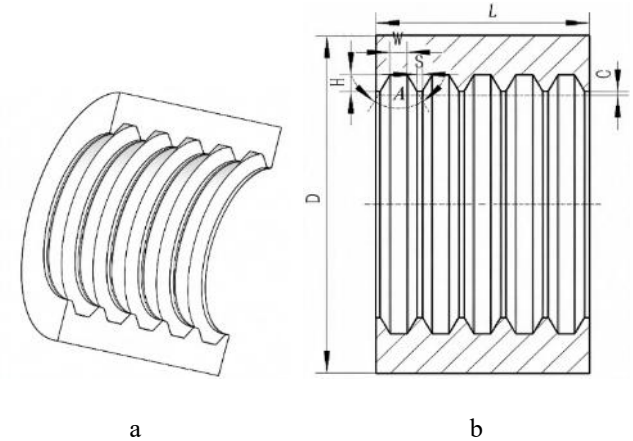

Fig. 4 Labyrinth sleeve: a – 3D model of labyrinth sleeve, b – 2D drawing of labyrinth sleeve

The preliminary geometric parameters of the labyrinth sleeve are calculated based on the theoretical formulas for labyrinth seal structural parameters [12]. The labyrinth sleeve has an outer diameter $D = 62$ mm and an overall length $L = 38$ mm, which is fitted with five trapezoidal throttling teeth. The tooth thickness $S = 1$ mm, tooth height $H = 3$ mm, tooth width $W = 3$ mm, the included angle between the two tooth sidewalls $A = 60°$ and the sealing clearance $C = 0.25$ mm.

2.2. Design of packing sealing structure

An inner stuffing box with stepped profile is added on the basis of the original stuffing box. This stepped structure enables the fluid pressure to decrease gradually from the high-pressure side to the sealing interface, so as to achieve superior sealing performance. An oil injection hole is arranged on the outer side of the outer stuffing box to

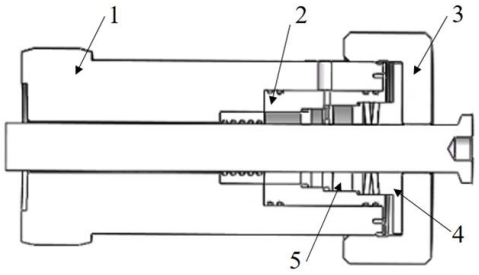

Fig. 5 Simplified model of composite sealing structure for plunger pump: *1* – outer stuffing box, *2* – inner stepped stuffing box, *3* – compression nut, *4* – gland, *5* – guide sleeve

mitigate abrasive wear between the packing and the plunger. Three guide sleeves are installed to avoid radial offset of the plunger. Meanwhile, disc springs are mounted on the low-pressure side of the inner stuffing box to realize automatic preload compensation for the packing assembly. The main components of this assembly include the outer stuffing box, stepped inner stuffing box, compression nut, gland and guide sleeves, and the three-dimensional geometric model of the overall composite sealing structure is shown in Fig. 5.

3. Numerical Simulation of Composite Sealing Structure for Plunger Pump

3.1. Numerical simulation analysis of labyrinth sealing structure

3.1.1. Selection of turbulence model

When adopting Fluent to conduct finite element analysis on the internal fluid field of trapezoidal labyrinth sealing structures, an appropriate turbulence model must be selected. A variety of turbulence models are available for numerical simulation, mainly including the standard k–ε model, RNG k–ε model, Realizable k–ε model, SST k–ε model and Reynolds Stress Model (RSM) [13]. Calculation results indicate that the Reynolds number inside the labyrinth seal is far higher than 4000. The standard k–ε model delivers high precision for fluids with large Reynolds numbers and exhibits favorable adaptability under low-Reynolds-number conditions [14]. Accordingly, the standard k–ε model is adopted in this paper for finite element simulation analysis.

3.1.2. Establishment of numerical model

The flow channel model is established according to the structural parameters of the labyrinth seal designed above. To improve the accuracy of calculation results, geometric simplification is performed without compromising computational validity, and the simplified model is displayed in Fig. 6.

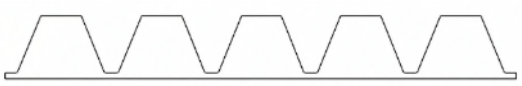

Fig. 6 Analysis model of labyrinth seal

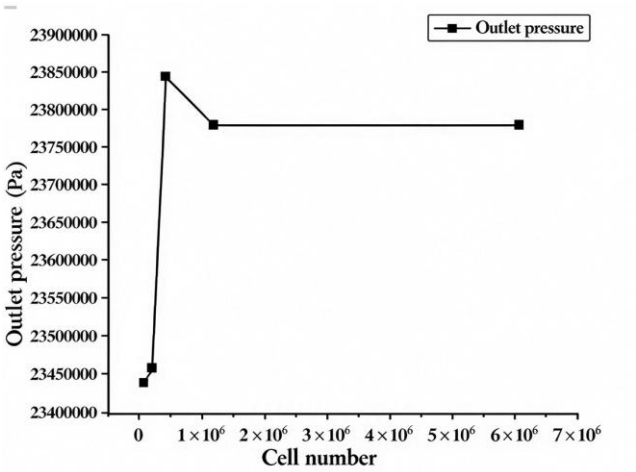

Fig. 7 Relationship between maximum outlet pressure and mesh quantity

3.1.3. Mesh independence verification

In the finite element fluid domain simulation via Fluent, the labyrinth seal model is meshed with five sets of grids featuring different element quantities: 115118, 206554, 424760, 1194643 and 6089749. The correlation curve between mesh quantity and outlet pressure of the labyrinth seal is plotted in Fig. 7.

It can be observed from Fig. 7 that the outlet pressure tends to stabilize when the mesh element count exceeds 1194643. Taking both simulation accuracy and computational efficiency into comprehensive consideration, the mesh scheme with 1194643 elements is finally adopted for the model discretization.

3.1.4. Solver parameters setup

Boundary conditions and relevant parameters are defined in the Setup module of Fluent. Firstly, mesh check is carried out on the fluid domain of the labyrinth seal to eliminate negative volume cells. The Pressure-Based solver is selected as the solution type, Absolute velocity is adopted for velocity formulation, steady-state flow is calculated, and the standard k–ε turbulence model is used for finite element simulation.

For the analysis setup of the labyrinth seal, liquid water (water-liquid) is specified as the working medium inside the fluid domain. The pressure-inlet boundary condition is assigned to the flow inlet with an inlet static pressure of 40 MPa, while the flow outlet is set as a pressure-outlet boundary with a static pressure of 0 Pa. Stationary walls with the no-slip shear condition are applied to all wall surfaces.

For solution methods, the SIMPLEC algorithm is chosen for pressure–velocity coupling. The second-order upwind scheme is adopted for the discretization of turbulent kinetic energy, Reynolds stress and other variables. The default under-relaxation factors are retained, and other relevant options are kept as default settings. Hybrid initialization is performed for the entire flow field, and the total number of iteration steps is set to 1000 to complete the computation.

3.1.5. Analysis of numerical simulation results

Fluent fluid simulation software is used to complete the numerical calculation of the flow field inside the labyrinth seal, and the simulated flow field characteristics of the labyrinth seal are presented in Fig. 8.

It can be seen from the pressure contour that fluid flows in from the left inlet of the labyrinth, and the fluid pressure decreases gradually with the minimum pressure at the outlet; the total pressure difference reaches 20.51 MPa, and drastic pressure variation occurs inside the grooves close to the inlet side.

As indicated by the velocity contour, the fluid velocity rises sharply before passing through the throttling clearance. This phenomenon arises because pressure energy is converted into kinetic energy when high-pressure fluid flows through labyrinth teeth into grooves, which reduces fluid pressure and accelerates flow velocity. In addition, the flow velocity near the groove walls is higher than that at the central region of the grooves.

The pathline diagram reveals that vortex zones are

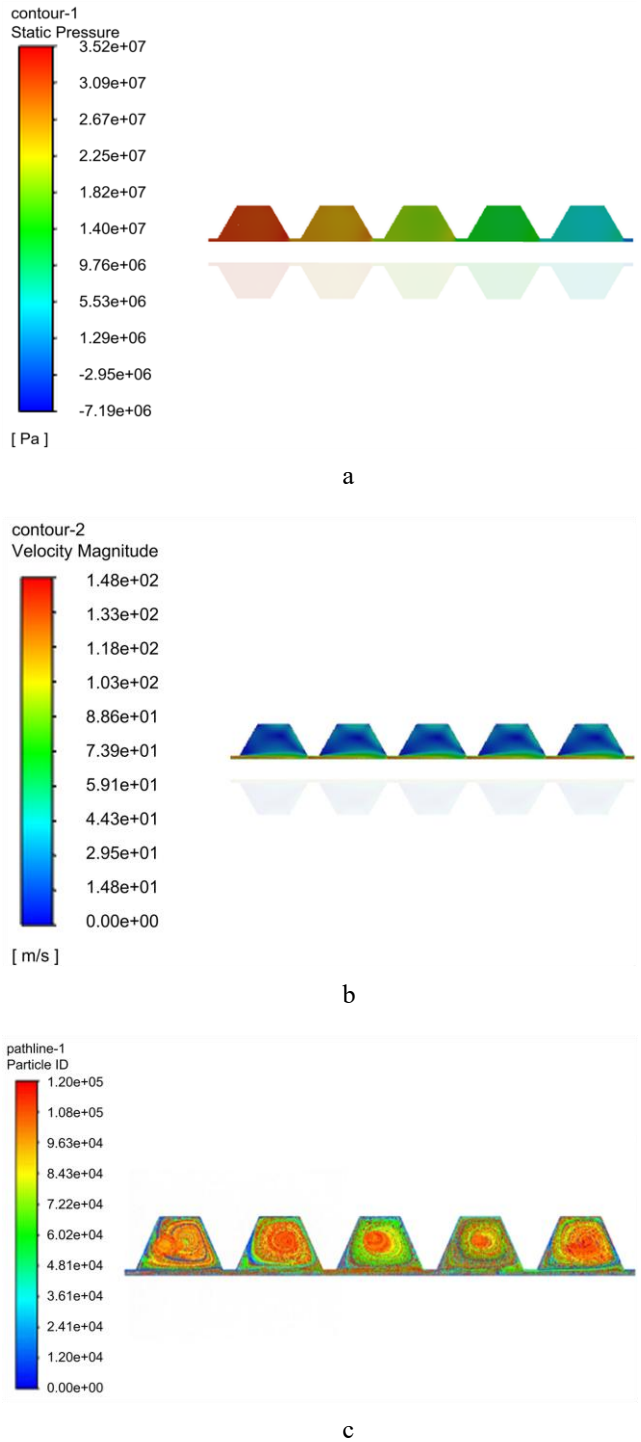

Fig. 8 Numerical simulation results of labyrinth seal: a – pressure contour, b – velocity contour, c – pathline diagram

generated in the middle of the five tooth grooves, demonstrating that partial kinetic energy drives the fluid to form vortices within labyrinth grooves.

In conclusion, the pressure of high-pressure liquid drops remarkably when flowing from the leftmost inlet to the rightmost outlet of labyrinth grooves. After passing through the full labyrinth sealing structure, the total pressure drop of liquid reaches 20.51 MPa, equivalent to a pressure reduction of approximately 50%. This reduces the bearing pressure of packing materials, alleviates the service load on packing seals, and significantly extends the service life of packing assemblies.

3.2 Numerical Simulation Analysis of Packing Sealing Structure

3.2.1 Determination of Packing Material Combination and Cross-Section Profile

The friction and wear properties of polytetrafluoroethylene, aramid and rubber are obtained through packing friction and wear tests [8]. Among the three packing materials, PTFE exhibits the optimal friction and wear resistance, followed by aramid, while rubber shows the worst tribological performance. Combined with practical field operation experience in oilfields, packing materials with high hardness, outstanding wear resistance and large lateral pressure coefficient are required on the high-pressure side. Hard and wear-resistant materials are also adopted at the low-pressure driving end where the packing is in direct contact with the gland, so that preload compression can be implemented conveniently. Accordingly, wear-resistant and rigid PTFE packing rings are arranged on the high-pressure side, aramid packing rings with moderate performance are installed on the low-pressure side for reliable sealing, and rubber packing rings with relatively inferior tribological properties are placed in the middle position.

Considering the high-pressure and high-speed service conditions as well as manufacturing difficulty, a combined assembly consisting of three stacked V-shaped sealing rings and three rectangular sealing rings is proposed in this work. The V-shaped packing assembly is placed on the high-pressure side, followed by rectangular packing rings. In this layout, the pressure of leaked fluid is gradually reduced when passing through each sealing ring, and the pressure is effectively dissipated before reaching the last sealing ring. This arrangement suppresses medium leakage and achieves optimal sealing performance. The overall assembly layout is illustrated in Fig. 9.

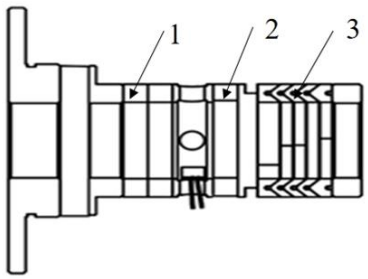

Fig. 9 Assembly sequence of packing rings inside the stuffing box: *1* – two aramid rectangular packing rings, *2* – rubber rectangular packing ring, *3* – stacked V-shaped PTFE packing assembly

3.2.2. Establishment of numerical model

The term "composite" adopted for the packing sealing structure in this study has two connotations: one refers to the sealing configuration formed by combining V-shaped rings and rectangular rings; the other corresponds to the relative layout, where the V-shaped ring assembly close to the high-pressure side serves as the primary sealing barrier and the rectangular ring assembly far from the high-pressure side acts as the secondary sealing barrier. The composite sealing structure contains auxiliary components such as guide sleeves and liquid injection rings. To simplify com-

putational simulation, only the influence of V-shaped packing rings on sealing performance is investigated in this section, and the schematic diagram of the corresponding structure is shown in Fig. 10.

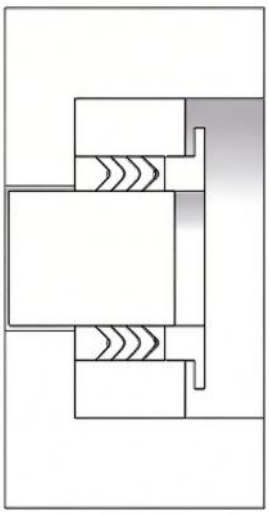

Fig. 10 Schematic diagram of V-shaped packing sealing structure

3.2.3. Mesh independence verification

The global mesh size of the entire packing sealing structure is set to 0.6 mm, while five different mesh sizes of 0.5 mm, 0.4 mm, 0.3 mm, 0.2 mm and 0.1 mm are assigned to the V-shaped packing model for simulation calculation. The equivalent stress of the packing ring is taken as the evaluation index for mesh independence verification, and the meshing diagram with a mesh size of 0.5 mm is presented in Fig. 11.



Fig. 11 Mesh generation diagram

The simulation results show that the maximum equivalent stresses of V-shaped packing rings under the five mesh sizes are 36.445 MPa, 36.014 MPa, 25.292 MPa, 22.444 MPa and 32.813 MPa respectively, and the distribution patterns of equivalent stress are basically consistent. To guarantee calculation accuracy and improve computational efficiency simultaneously, a mesh size of 0.5 mm is adopted for the V-shaped packing ring in subsequent numerical simulations.

3.2.4. Solver parameters setup

Two load steps are defined in the finite element analysis. In the first load step, full fixed constraints are imposed on the plunger and stuffing box, and a 2 mm displacement load is applied on the gland to simulate the pre-compression process and realize the preloading working condition. On the basis of the preloading state in the second load step corresponding to pressure-bearing operation, a fluid pressure of 20 MPa is loaded on the packing surface at the high-pressure side.

3.2.5. Analysis of numerical simulation results

When evaluating the performance of packing sealing structures, equivalent stress is commonly adopted to assess the overall yielding risk of packing materials and judge whether sealing failure occurs due to excessive deformation; shear stress is used to identify potential tearing or shear fracture induced by excessive shear load; frictional stress reflects the friction and wear degree of materials so as to avoid medium leakage and performance deterioration; contact stress is employed to check whether the maximum contact pressure on sealing interfaces exceeds the fluid medium pressure, which further determines the sealing reliability.

ANSYS software is utilized to conduct numerical simulation analysis on the packing sealing assembly, and the simulated cloud contours are displayed in Fig. 12.

As illustrated in Fig. 12, the maximum equivalent stress of the packing ring reaches 35.749 MPa and appears at the tip of the inner inclined lip, which indicates that the lip tip is the most vulnerable to damage. The maximum positive shear stress of the packing is 12.569 MPa, located on the left side of the V-shaped inner angle, while the maximum negative shear stress emerges at the symmetrical position on the right side. The maximum contact stress of the packing is 27.545 MPa at the contact interface between the packing and the inner stuffing box. The peak contact pressure of all packing rings exceeds the operating medium pressure, satisfying the sealing performance requirements. The maximum frictional stress of the packing is 5.9095 MPa, which distributes on the left area of the V-shaped packing ring.

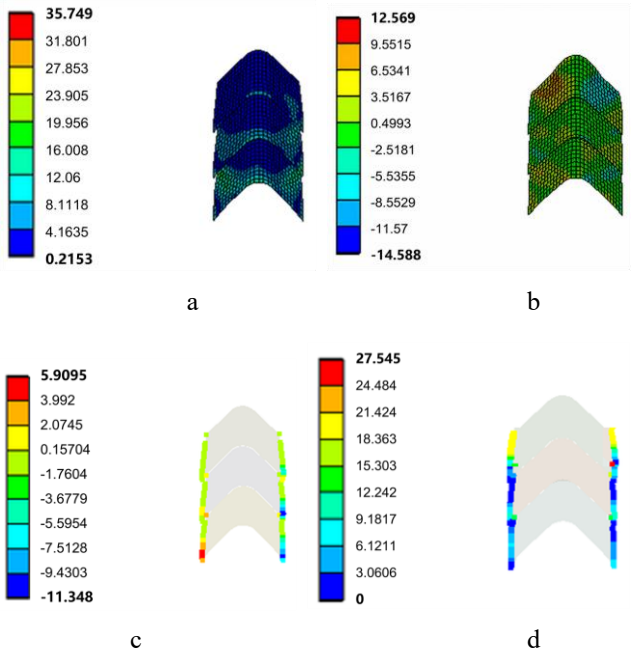

Fig. 12 Cloud contours of numerical simulation results for packing seals: a – equivalent stress contour, b – shear stress contour, c – frictional stress contour, d – contact stress contour

Contact stress values on the interfaces between the packing and plunger as well as between the packing and inner stuffing box are extracted, sorted and plotted into contact stress curves, as shown in Fig. 13, a and b.

It can be seen from Fig. 13 that the maximum contact stress between the plunger and packing surface is 27.545 MPa, and the maximum contact stress between the packing and inner stuffing box surface is 22.6 MPa, both of which can prevent medium leakage. In conclusion, the maximum contact stress on the interfaces of packing-plunger and packing-inner stuffing box is higher than the medium pressure of 20 MPa, which verifies the reliable sealing capacity of the proposed packing structure.

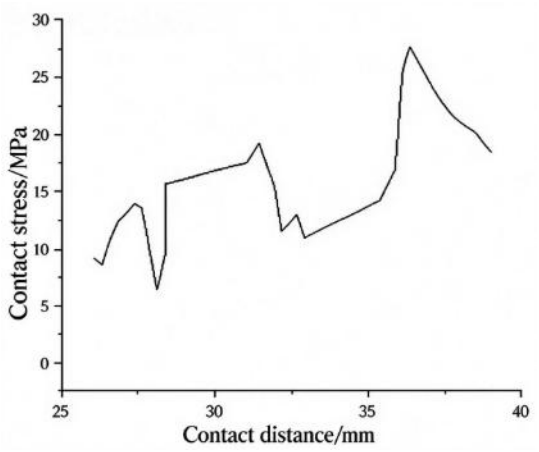

a

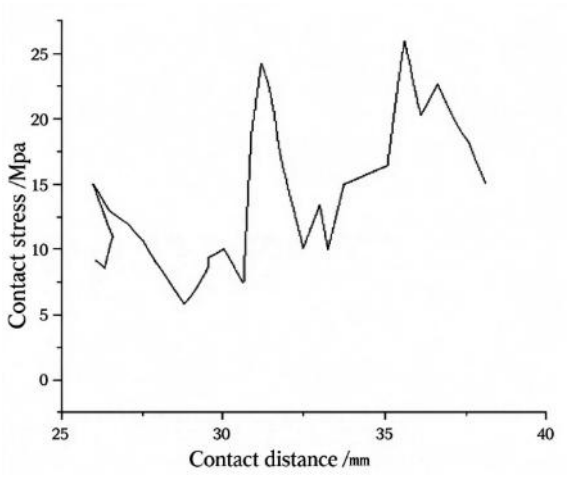

b

Fig. 13 Contact stress distribution curves: a – contact stress curve of plunger-packing interface, b – contact stress curve of packing-inner stuffing box interface

4. Parameter Optimization of V-Shaped Packing Ring

4.1. Single-factor analysis

According to literature investigation on single-factor analysis of V-shaped packing structures, several geometric parameters are selected for single-factor research. The height and radial thickness of the V-shaped packing ring are denoted as s and *r*, respectively; the lip inclination angle of the V-shaped packing ring is defined as variable α; the rear lip included angle and front lip included angle of the V-shaped packing ring are represented by β and γ; and the interference fit magnitude of the V-shaped packing ring is marked as δ. Single-factor simulation re-search is carried out on the above six structural parameters, and the cross-sectional schematic of each geometric parameter is presented in Fig. 14.

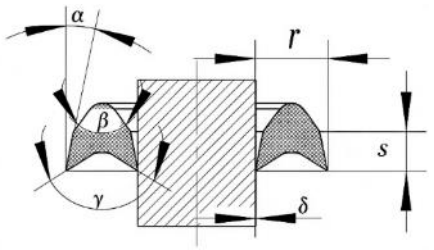

Fig. 14 Cross-sectional schematic of V-shaped packing ring structure

Single-factor numerical simulation analysis is performed for the six structural variables of the V-shaped packing ring to explore the influence laws of different geometric parameters on its sealing characteristics.

The single-factor numerical simulation results of V-packing are collated, and the simulation results under different V-packing heights are listed in Table 1. The simulation results for different radial thicknesses are listed in Table 2. The simulation results under different lip inclination angles are presented in Table 3.

The simulation results for different rear lip included angles are shown in Table 4. The simulation results under different front lip included angles are summarized in Table 5. The simulation results of V-shaped packing rings with different interference magnitudes are sorted in Table 6.

After comprehensively considering the influences of single factors on equivalent stress, shear stress, frictional stress and contact stress, the radial thickness of 10.5 mm and

Table 1

Data results for various packing ring heights

s, mm	Maximum equivalent stress, MPa	Maximum shear stress, MPa	Maximum frictional stress, MPa	Maximum contact stress, MPa
4	30.591	11.081	14.636	58.545
4.5	22.811	7.616	14.316	57.263
5	25.673	8.654	7.663	44.994
5.5	35.749	11.145	5.909	61.926
6	27.984	13.739	6.159	44.14

Table 2

Data results for various radial thicknesses

r, mm	Maximum equivalent stress, MPa	Maximum shear stress, MPa	Maximum frictional stress, MPa	Maximum contact stress, MPa
9	29.401	8.336	7.039	39.430
9.5	28.957	10.054	7.556	40.057
10	28.597	8.722	8.009	49.252
10.5	26.275	9.520	8.196	53.342
11	25.181	9.500	13.336	69.123

Table 3

Data results for various lip inclination angles

α, mm	Maximum equivalent stress, MPa	Maximum shear stress, MPa	Maximum frictional stress, MPa	Maximum contact stress, MPa
0	10.537	5.7682	2.176	24.934
1	12.497	6.7437	4.605	32.172
2	26.533	12.671	7.264	35.137
3	44.732	14.37	7.073	33.179
4	41.752	16.038	7.162	32.083

Table 4

Data results for various rear lip included angles

β, mm	Maximum equivalent stress, MPa	Maximum shear stress, MPa	Maximum frictional stress, MPa	Maximum contact stress, MPa
90	20.984	7.820	3.47	23.946
93	32.356	11.711	6.10	31.27
95	36.677	12.744	5.71	25.65
98	39.041	13.927	6.09	27.610
100	39.332	18.829	7.76	31.060

Table 5

Data results for various front lip included angles

γ, mm	Maximum equivalent stress, MPa	Maximum shear stress, MPa	Maximum frictional stress, MPa	Maximum contact stress, MPa
85	29.54	9.94	8.56	34.25
88	32.87	13.75	6.18	44.93
90	20.98	7.82	3.48	23.95
93	22.63	8.64	3.61	23.66
95	23.89	12.62	3.82	28.18

Table 6

Data results for various interference magnitudes

δ, mm	Maximum equivalent stress, MPa	Maximum shear stress, MPa	Maximum frictional stress, MPa	Maximum contact stress, MPa
0	41.76	14.23	6.30	29.34
0.05	41.81	13.49	6.51	31.28
0.1	40.56	17.37	8.04	32.18
0.15	42.72	13.36	2.87	25.87
0.2	44.14	10.78	5.60	22.38

interference magnitude of 1 mm are determined. Four structural parameters to be optimized for the V-shaped packing ring are the packing height s, lip inclination angle α, rear lip included angle β and front lip included angle γ. Three levels are selected for each parameter, and an orthogonal optimization design with four factors and three levels is carried out.

4.2. Optimization analysis

To determine the optimal structural parameter combination of the V-shaped packing, the orthogonal test method is adopted for parameter optimization analysis in this paper. Compared with the comprehensive test method, the orthogonal test can screen typical and representative parameter combinations, greatly reducing the test workload while ensuring reliable results [15]. A total of 18 groups of orthogonal tests are designed and carried out.

The Min-Max deviation normalization method is used to perform linear transformation on the original test data to unify the dimensions of each evaluation index. The maximum contact stress is taken as a positive index, while the maximum equivalent stress, maximum shear stress and maximum frictional stress are taken as negative indices. Data preprocessing for the two types of indices is carried out using the formulas given below

$$b_{ij} = \frac{x_{ij} - min(x_i)}{max(x_i) - min(x_i)}, \tag{1}$$

$$b_{ij} = \frac{max(x_i) - x_{ij}}{max(x_i) - min(x_i)}, \tag{2}$$

where: b_{ij} is the normalized value, x_{ij} is the raw data of orthogonal test results.

After data preprocessing, the entropy weight method is employed to calculate the weight of each evaluation index so as to determine the optimal parameter combination. First, the contribution degree of different schemes under positive and negative indices is calculated via the following formula. Then, the entropy values of the four indices are calculated according to the entropy formula, which are 0.945, 0.964, 0.956 and 0.866, respectively.

$$p_{ij} = \frac{b_{ij}}{\sum_{i=1}^{m} b_{ij}}, \tag{3}$$

where: p_{ij} is the contribution degree of the i-th scheme under the j-th index.

$$E_j = -k \sum_{i=1}^{n} p_{ij} \, ln \, p_{ij}, \tag{4}$$

where: $k = 1/ln_n$; $0 \le p_{ij} \le 1$ and $\sum_{i=1}^{n} p_{ij} = 1$. If $p_{ij} = 1$, we define $\lim_{p_{ij} \to 0} p_{ij} \, ln \, p_{ij} = 0$.

On the basis of the above entropy values of indices, the consistency degree of each index is further calculated by the following formulas, and the results are 0.055, 0.036, 0.044 and 0.134, respectively.

$$d_j = 1 - E_j. \tag{5}$$

Finally, the weight coefficients of the four indices are obtained using the weight formula, which are 0.203, 0.134, 0.165 and 0.498, respectively

$$W_j = \frac{d_j}{\sum_{j=1}^{m} d_j}. \tag{6}$$

Combined with the weight of each index, the multi-index comprehensive evaluation model for the V-shaped

packing structure is established as follows:

$$K = 0.203 \times DX + 0.134 \times JQ + \\ +0.165 \times MC + 0.498 \times JC \quad , \tag{7}$$

where: DX is the equivalent stress, JQ is the shear stress, MC is the frictional stress, JC is the contact stress.

Visual analysis is conducted on the K-values obtained from the orthogonal test results, and the analytical results are listed in Table 7.

Analysis of variance (ANOVA) is performed on the test results, and the analytical results are listed in Table 8.

From the F-test based on the ANOVA table of orthogonal test, it can be obtained that the critical value λ equals 3.26 at the significance level $\alpha = 0.10$. The F-values of all factors are greater than 3.26, indicating that all factors exert significant effects on the evaluation index K. The sequence of significance is consistent with the results from visual analysis of orthogonal test data. Based on the visual analysis and variance analysis of the orthogonal test, the optimal combination of structural parameters for the V- shaped packing ring is determined as A3, B3, C3, D1.

Table 7

Visual analysis table of orthogonal test

Factor	A	B	C	D	E
K1	20.109	16.699	22.427	24.677	24.112
K2	22.337	23.410	19.136	21.378	22.486
K3	24.495	26.840	25.377	20.885	20.342
R	4.386	10.141	6.241	3.792	3.770
Optimal level	A3	B3	C3	D1	E1
Order of significance	3	1	2	4	5

Table 8

Analysis of variance table for orthogonal test

Source	Sum of square	DF (degrees of freedom)	Mean square	F-value	Significance
Factor A	9.619	2	4.809	4.708	Significant
Factor B	53.196	2	26.597	26.035	Highly significant
Factor C	19.493	2	9.747	9.541	Significant
Factor D	8.504	2	4.252	4.162	Significant
Error	7.151	7	1.022	—	—
Total	97.960	17	—	—	—

Table 9

Optimized parameters of V-shaped packing ring

Factor	Packing height s	Lip inclination angle α	Rear lip included angle β	Front lip included angle γ
Parameter	5 mm	4°	98°	90°

Accordingly, the specific optimized parameters of the V-shaped packing ring are shown in Table 9.

4.3. Numerical simulation analysis of optimized packing sealing structure

Numerical simulation analysis of the optimized packing sealing structure is carried out using ANSYS software, and the simulation results are shown in Fig. 15.

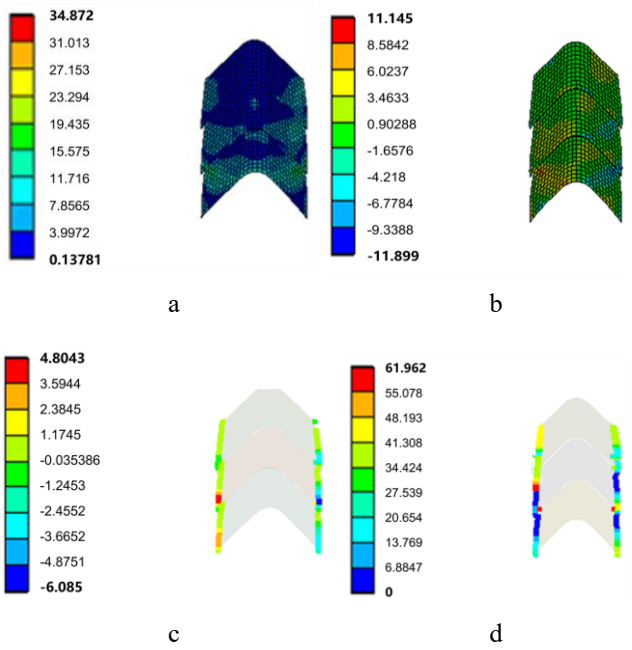

Fig. 15 Contour plots of numerical simulation results for the packing seal: a – equivalent stress contour, b – shear stress contour, c – frictional stress contour, d – contact stress contour

A comparison between the simulation results before and after optimization reveals that the equivalent stress and shear stress of the packing ring decrease slightly, which means cracks and plastic deformation are less likely to emerge in the packing material. Meanwhile, the contact stress of the packing ring rises correspondingly, and the frictional stress is slightly lower than that before optimization. It demonstrates that the sealing performance of the packing ring is further improved after optimization.

5. Indoor Test Verification

To investigate the practical performance of the optimized novel combined sealing structure of plunger pump under actual working conditions, and to evaluate the validity and reliability of the foregoing numerical simulation results, indoor tests are carried out based on the prototype with structural parameters of the optimized plunger pump combined seal. The tests include two parts: first, the pressure reduction characteristic test of the labyrinth sleeve to verify the pressure drop under specified inlet pressure; second, the contact stress test of the packing seal under assembly conditions to verify the contact stress between the plunger and the packing.

5.1. Labyrinth pressure reduction characteristic test

The test rig for labyrinth pressure reduction characteristics consists of a labyrinth sleeve, inlet and outlet pressure gauges, a centrifugal pump, and a water tank. The physical photo of the test pipeline built in this work is shown in Fig. 16.

By adjusting the inlet pressure regulating valve of the test section, the readings of the inlet pressure gauge are set to 0.04 MPa, 0.08 MPa, 0.12 MPa, 0.16 MPa and 0.2 MPa, respectively. Experiments are performed to measure the outlet pressure, and the corresponding experimental pressure drops are acquired to verify the accuracy of simulation results.

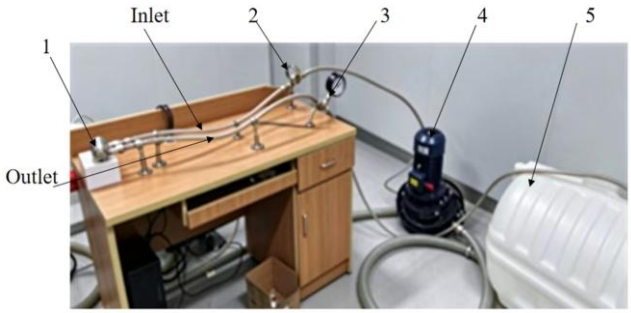

Fig. 16 Physical photo of the test pipeline: *1* – labyrinth sleeve, *2* – inlet pressure gauge, *3* – outlet pressure gauge, *4* – centrifugal pump; *5* – water tank

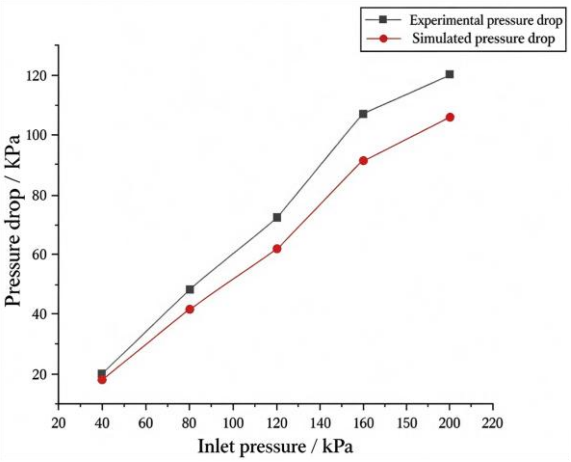

Fig. 17 Statistical diagram of inlet pressure versus pressure drop

As illustrated in Fig. 17, the pressure drop error between experimental measurements and numerical simulation is less than 15%, which falls within the allowable error range and verifies the effectiveness of finite element simulation. Meanwhile, calculation from experimental data indicates that the pressure of high-pressure water decreases by approximately 50% after flowing through the labyrinth channel. This demonstrates the correctness of the pressure-drop flow law inside the labyrinth channel and verifies the feasibility of the scheme adopting a labyrinth sleeve to reduce the sealing pressure of the combined packing seal.

5.2. Contact stress test of packing seal

The overall test rig consists of a hydraulic press, combined packing sealing structure, strain gauges and a network data acquisition instrument. The schematic of the complete test setup is shown in Fig. 18.

The hydraulic press is activated to control the reciprocating displacement of the plunger at 180 mm. The plunger performs periodic up-and-down reciprocating motion with a cycle of 11 minutes. The above test procedure is repeated three times, and the average value of measured results is adopted.

A comparison between experimental results and simulation data is illustrated in Fig. 19.

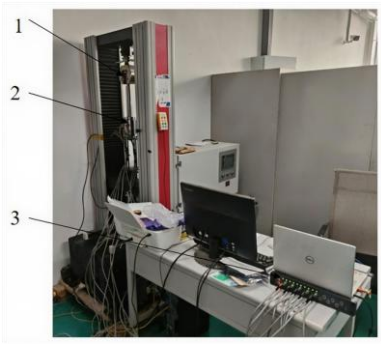

Fig. 18 Schematic of the overall test setup: *1* – hydraulic press, *2* – combined packing sealing structure (with strain gauges attached), *3* – network data acquisition instrument

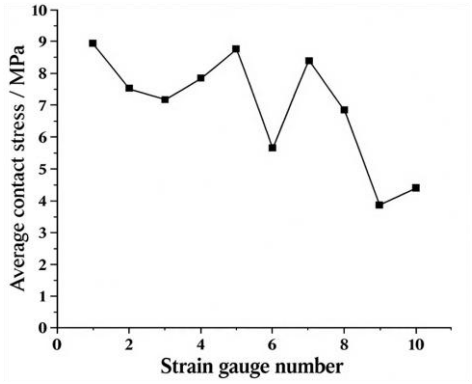

a

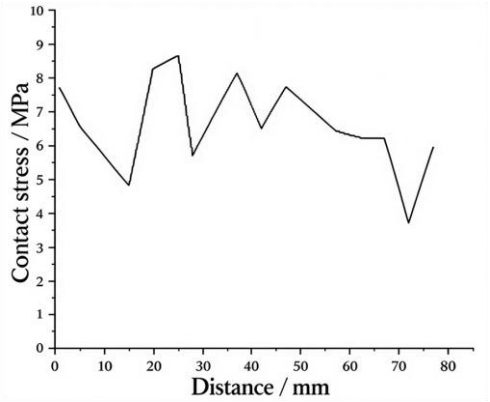

b

Fig. 19 Axial stress distribution diagrams: a – axial distribution of experimental contact stress, b – axial distribution of simulated contact stress

By comparing Fig. 19, a and b, the axial distribu-

tion of packing contact stress obtained from experiments basically agrees with finite element simulation results, and the deviation is within 10%, falling within the allowable error range. This proves the accuracy of finite element simulation analysis.

6. Conclusions

A novel combined sealing structure for plunger pumps is proposed. Three-dimensional models of the labyrinth seal and V-packing seal are established, and investigations are carried out combining finite element simulations and laboratory tests. Numerical simulations are adopted to analyze the internal flow characteristics of the labyrinth, and the influence laws of the height, thickness, front lip angle, rear lip angle and interference of V-packing on sealing performance are explored. The main conclusions are summarized as follows:

The stepped inner stuffing box and trapezoidal-tooth labyrinth structure are designed, and the preliminary geometric dimensions of the novel combined sealing structure for plunger pumps are determined.

Flow simulations of the labyrinth seal are conducted using Fluent. The results reveal that the pressure drops by approximately 50% after the medium flows through the labyrinth, which effectively reduces the pressure borne by the packing. Simulations of the V-packing demonstrate that the original structure meets the sealing requirements.

A total of 30 sets of single-factor simulation analyses for the V-packing are performed via ANSYS to obtain the optimal level of each structural parameter. Eighteen groups of orthogonal tests are designed, the weights of evaluation indicators are determined based on the entropy weight method, and a multi-index comprehensive performance evaluation model is established. The optimal parameter combination is obtained: height $s = 5$ mm, lip inclination angle $\alpha = 4°$, rear lip angle $\beta = 98°$, front lip angle $\gamma = 90°$. Further simulations verify that the sealing performance of the optimized V-packing is improved.

A test platform is built to carry out laboratory tests. The maximum error between labyrinth pressure drop test data and simulation results is less than 15%, which verifies the feasibility of reducing the pressure acting on the packing via the labyrinth structure. The maximum error of contact stress between test measurements and simulation predictions for V-packing is 10%, which proves the reliability of numerical simulations and the effectiveness of structural optimization.

References

1. **Du, M. J.; Xi, J. Q.; Liu, Y. P.; Hou, Y. J.; Li, H. C.; Yang, X. P.; Wang, Z. X.; Dai, Q. P.; Duan, P.; Zhao, M. J.; Jiang, S. K.** 2023. Design of three-stage sealing structure and investigation of sealing performance for 7000 fracturing plunger pump, Mechanika 29(1): 19-26. https://doi.org/10.5755/j02.mech.31091.
2. **Yin, T. Y.; Wei, D. S.; Suo, S. F.** 2021. Discussion on measurement technology of friction force for reciprocating seals, Lubrication Engineering 46(09): 143-153 (in Chinese). https://doi.org/10.3969/j.issn.0254-0150.2021.09.021.
3. **Peng, C. T.; Zhang, J.; Zhou, Z. Y.; Hao, J. S.; Jiang, Q. B.; Chang, L. D.; Yang, R.** 2023. Experimental study on friction, wear and sealing performance of graphite packing, Lubrication Engineering 48(12): 194-200 (in Chinese). https://doi.org/10.3969/j.issn.0254-0150.2023.12.026.
4. **Jin, X. L.; Zhang, L. Z.; Ni, Y.** 2023. Structural improvement and sealing performance research of flexible graphite packing, Lubrication Engineering 48(03): 164-170 (in Chinese). https://doi.org/10.3969/j.issn.0254-0150.2023.03.022.
5. **Luo, L. J.; He, X. F.; Liu, X.; Zhang, Q. X.; Huang, H. W.** 2024. Design of experimental device for plunger sealing performance of water hydraulic pump, Chinese Journal of Mechanical Engineering 35(02): 229-235 (in Chinese). https://doi.org/10.3969/j.issn.1004-132X.2024.02.006.
6. **Zhang, M.; Wang, Q. X.; Ren, C.; Meng, X. P.** 2012. Structural improvement of packing seal for high-pressure plunger pump, Plant Maintenance Engineering (08): 56-57 (in Chinese). https://doi.org/10.3969/j.issn.1001-0599.2012.08.030.
7. **Zhu, C. Z.; Zhu, H. B.; Sheng, W. B.; Song, J.** 2022. Improvement and effect analysis of packing sealing mode for water injection pump plunger, Mechanical Engineer (05): 53-54+57 (in Chinese).
8. **Xu, M. M.; Kong, J.; Li, F.; Wang, X. J.; Zhang, J.** 2025. Experimental study on the influence of packing materials on plunger sealing performance, Mechanical & Electrical Engineering Technology 54(05): 123-127 (in Chinese). https://doi.org/10.3969/j.issn.1009-9492.2025.05.022.
9. **Pipper, F**. 1999. Handling hostile environments at a stroke, Sealing Technology 1999(61): 6-8. https://doi.org/10.1016/S1350-4789(00)80181-6.
10. **Wang, Y. C.; Zhang, X. H.; Sun, C. Q.; Deng, J. L.** 2024. Optimal design and manufacturing of labyrinth trim for 3D printed regulating valve, Special Casting & Nonferrous Alloys 44(06): 791-796 (in Chinese). https://doi.org/10.15980/j.tzzz.2024.06.011.
11. **Jin, H. Z.; Duan, A. Q.; Liu, X. F.; Wang, C.** 2022. Flow pressure reduction characteristics and critical cavitation prediction of straight-through labyrinth regulating valve flow channel, Journal of Drainage and Irrigation Machinery Engineering 40(09): 921-927 (in Chinese).
12. **Fan, Z. M.; Wang, Q. L.; Li, L.** 2019. Design and analysis of combined sealing structure for deep sea piston pressure balancer, Lubrication Engineering 44(06): 95-100 (in Chinese). https://doi.org/10.3969/j.issn.0254-0150.2019.06.015.
13. **Veríssimo, A.; Oliveira, R.; Coelho, P. J.; Costa, M.** 2012. Numerical simulation of a small-scale mild combustor, Journal of Physics: Conference Series 395: 012003. https://doi.org/10.1088/1742-6596/395/1/012003.
14. **Li, Z. G.; Chen, Y. S.** 2012. Numerical analysis and research on flow field and leakage of labyrinth seal, Turbine Technology 54(6): 401-403+428 (in Chinese).
15. **Guo, J. X.; Guo, Z. P.; Cai, X. Y.; Wang, Z. J.; Sun, Q. T.; Niu, F. L.; Wang, S. F.** 2021. Research on suppression characteristics of pressure suppression pool based on orthogonal test, Nuclear Science and Engineering 41(4): 838-843 (in Chinese). https://doi.org/10.3969/j.issn.0258-0918.2021.04.024.

X. J. Zhou, J.J. Zhang, F. Li, H. R. Wang, Y. Wang

DESIGN AND PERFORMANCE INVESTIGATION OF A NOVEL COMPOSITE SEALING STRUCTURE FOR PLUNGER PUMPS

S u m m a r y

To tackle the problems of easy leakage, short service life and rapid wear failure of conventional packing seals for plunger pumps, this paper investigates a combined sealing structure. A labyrinth–V-packing combined sealing structure is proposed, and its three-dimensional model is established. Numerical simulations and experiments are used to explore the influence of V-packing structural parameters on sealing performance. Firstly, the structural scheme with a trapezoidal-tooth labyrinth seal on the high-pressure side and a stepped inner stuffing box is determined, and the preliminary design of the combined seal is finished. Secondly, Fluent is utilized to analyze the flow characteristics of the labyrinth seal. Based on the confirmed packing arrangement and cross-sectional profile, single-factor analysis and orthogonal experimental design are adopted to optimize V-packing parameters. Finally, test fixtures are fabricated and a test platform is set up to conduct labyrinth pressure drop tests and contact stress measurements. Experimental results reveal that the maximum error of labyrinth pressure drop between measured data and simulation results is 15%, and roughly 50% pressure reduction can be realized. The contact stress error between the plunger and V-packing is less than 10%. These results verify the reliability of numerical simulations and validate the effectiveness of the structural design and parameter optimization scheme of the proposed combined sealing structure.

Keywords: plunger pump, combined sealing structure, V-packing, labyrinth seal, orthogonal experimental method.

Received July 27, 2026
Accepted October 15, 2026

This article is an Open Access article distributed under the terms and conditions of the Creative Commons Attribution 4.0 (CC BY 4.0) License (http://creativecommons.org/licenses/by/4.0/).